Journal of Solid State Chemistry **144,** 437–441 (1999)
Article ID jssc.1999.8202, available online at http://www.idealibrary.com on IDEAL®

Preparation and Characterization of Garnet Phosphor Nanoparticles Derived from Oxalate Coprecipitation

Teng-Ming Chen,[1] S. C. Chen, and Chao-Jung Yu

Department of Applied Chemistry, National Chiao-Tung University, Hsinchu 300, Taiwan

Received October 7, 1998; in revised form February 2, 1999; accepted February 5, 1999

Terbium-activated $Y_3Al_5O_{12}$ (YAG:Tb) phosphor nanoparticles with homogeneous grain size and crystallinity have been prepared at 1000°C by heat treatment of a metal oxalate precursor derived from an alkaline coprecipitation route. The diffraction profile of as-prepared YAG:Tb nanoparticles can be indexed as a garnet structure and exhibits peak broadening phenonmenon, as revealed by X-ray diffraction (XRD) data. Grains of YAG:Tb nanoparticles appear to be irregularly spherical or elliptical and their sizes range from 60 to 70 nm, as indicated by morphological studies from bright-field transmission electron microscopy (TEM) imaging. Furthermore, the photoluminescence (PL) spectra of the $(Y_{2.9}Tb_{0.1})Al_5O_{12}$ phase were investigated to determine the energy level of electron transition related to luminescence processes and the possible blue shift in the excitation or emission PL spectra. © 1999 Academic Press

Key Words: **$(Y, Tb)_3Al_5O_{12}$; phosphor nanoparticles; oxalate coprecipitation; photoluminescence.**

INTRODUCTION

Rare-earth activated $Y_3Al_5O_{12}$ (YAG:R) garnet phases have shown considerable potential as rugged phosphors and scintillation materials because they exhibit a thermally stable lattice, a well-determined crystal structure and, most importantly, they resist saturation at high current excitation (1–3). At high electron excitation power densities (P), the light emitted from phosphors generally levels off, mainly due to material heating and the associated luminescence quenching problems (1). For instance, the cathodoluminescence (CL) intensity of $^5D_4$ emission ($\lambda = 544$ nm) of epitaxial YAG films doped with Tb^{3+} was observed to be nonlinear as a function of P under electron bombardment (2). The CL intensity of the YAG:Tb specimens exhibit deviation from linearity and saturate at P exceeding 10^4 watt/m^2, corresponding to an excitation current density of 3×10^{-3} amp/cm^2 (2, 3). On the other hand, YAG:R phosphors are typically synthesized by solid-state reactions between component oxides with or without fluxes, which generally require prolonged heat treatment at elevated temperature and repeated grinding or milling to assure product purity and composition homogeneity (4, 5). Other routes leading to the formation of various R-doped YAG's have also been investigated extensively, namely, coprecipitation (6, 7), sol–gel (8, 9), chemical vapor deposition (10), and thermal pyrolysis of metallorganic precursors (11). On the other hand, nanoparticles of yttrium iron garnet (YIG) were recently synthesized by thermal pyrolysis of ethylene glycol/citrate gel precursors (12), but the preparation of nanostructured phosphors for potential commercial applications has rarely been investigated and related synthetic conditions were not well established. Bhargava *et al.* reported nanocrystals of Mn-doped ZnS with sizes varying from 3.5 to 7.5 nm that can yield both high luminescent efficiencies and exhibit significant lifetime shortening (13). On the other hand, Zhang *et al.* prepared nanocrystalline Y_2SiO_5:Eu and discovered that both luminescent intensity and quenching concentrations of Eu^{3+} were enhanced in Y_2SiO_5:Eu nanoparticles (14). Our research interests in synthesizing YAG:Tb nanophases are motivated by the attempt to improve the luminescence efficiency and study the variation of lifetime of phosphors used for cathode ray tube (CRT) screens and high-definition projection television (HDTV).

Among the large number of YAG:R phosphors reported, Tb^{3+} has long been selected as an activator mainly because of its simple structure of ground and excited energy levels (15). Concentration quenching (16) and cross-relaxation effects (17) in the YAG:Tb system have also been thoroughly investigated. In this paper we demonstrate a methodology for the synthesis of a series of YAG:Tb phases and report the microstructure and photoluminescence (PL) spectra of the as-prepared YAG:Tb nanoparticles on the basis of investigations on X-ray diffraction (XRD), transmission electron microscopy (TEM), and PL spectroscopy.

[1]To whom correspondence should be addressed.

0022-4596/99 $30.00

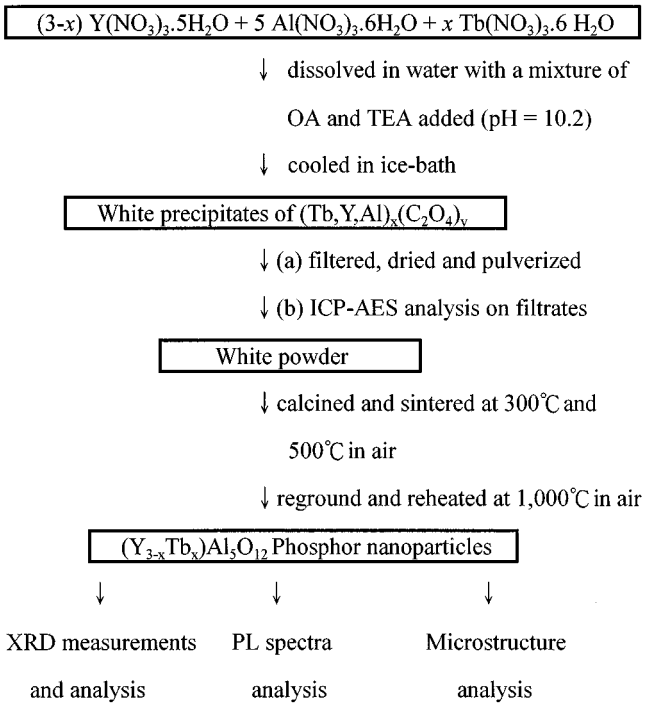

FIG. 1. Synthesis of $(Y_{3-x}Tb_x)Al_5O_{12}$ phosphor nanoparticles by alkaline oxalic acid (OA)-triethylamine (TEA) coprecipitation.

SYNTHESIS OF YAG:Tb PHOSPHORS

High-purity $Tb(NO_3)_3 \cdot 6H_2O$, $Y(NO_3)_3 \cdot 5H_2O$ and $Al(NO_3)_3 \cdot 6H_2O$ with a cationic molar ratio for Tb:Y:Al of $x:(3-x):5$ $(0.05 < x < 3)$ and 2.5 mmol of Y^{3+} were dissolved in 25 ml deionized water. An aqueous solution of coprecipitant was prepared by dissolving 0.025 mol of oxalic acid (OA) in 10 ml of deionized water. The pH of OA solution was then adjusted to an optimal value of 10.2 by adding 25 ml of triethylamine (TEA). The solution of the metal nitrates was then added dropwise into the OA–TEA solution with vigorous stirring. During mixing a white precipitate formed and the solution was then cooled in an ice-water bath. After separation of the precipitate and filtrate, the white gel-like precipitate was then dried and the obtained precipitate was subsequently calcined at 300°C followed by another thermal treatment at 500°C for 1 h, respectively, and then sintered at 1000°C for 24 h in air. The preparation of YAG:Tb nanoparticles is summarized in a flow diagram and represented in Fig. 1. The resulting fine powder used for XRD, TEM imaging, and PL spectra measurements was obtained by milling the calcined products with a Retsch MM 2000 mixer mill.

The X-ray diffraction (XRD) patterns of Tb-doped YAG phases were measured on a MAC Science MXP-3 automatic diffractometer using graphite-monochromatized and Ni-filtered Cu$K\alpha$ radiation. The specimens for bright-field transmission electron microscopy (TEM) were obtained by ultrasonically dispersing the nanoparticles in ethanol, and dispersed drops of the specimens were then transferred onto a Cu grid covered with a carbon film. Subsequently, the morphological studies were carried out on a Hitachi H-600 electron microscope operating at 100 kV and with a magnification of ca. 100,000X. The PL spectra of as-prepared

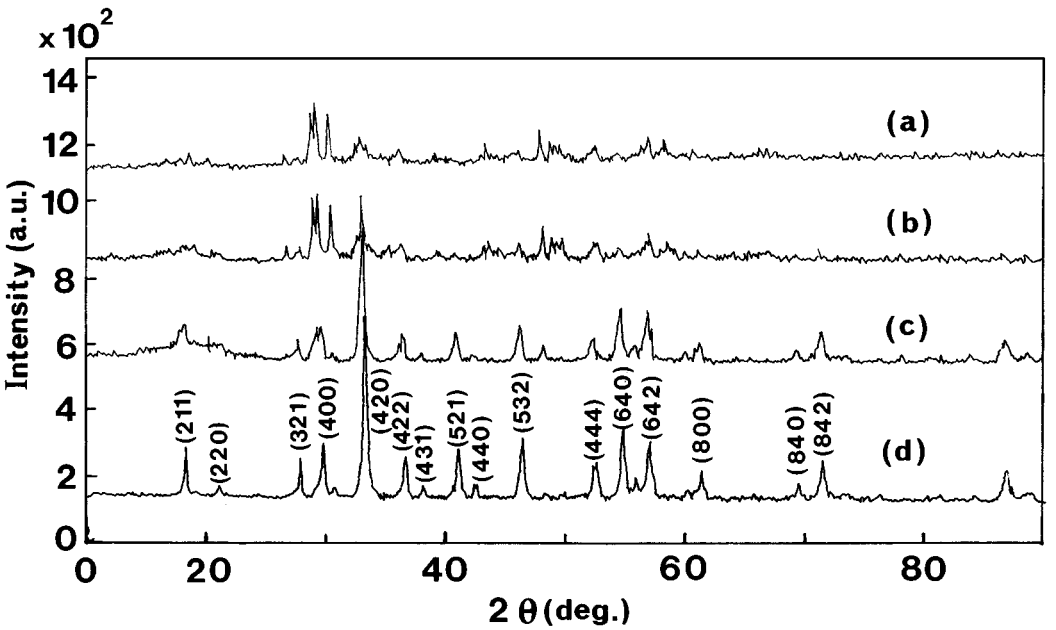

FIG. 2. The XRD pattern of products derived from calcination and sintering of metal oxalate coprecipitates for (a) 12 h, (b) 16 h, (c) 20 h, and (d) 24 h, respectively.

Tb-doped YAG nanoparticles were measured by using a Shimadzu RF-5301PC spectrofluorophotometer. The chemical compositions of cations in both precipitates and filtrates were checked with a Perkin Elmer SCIEX ELAN 500 inductively coupled plasma atomic emission spectrometer (ICP-AES).

A series of $(Y_{3-x}Tb_x)Al_5O_{12}$ phases with $0.05 < x < 3.0$ were prepared from an oxalate precursor derived from an alkaline coprecipitation route with an optimal pH of 10.2 and at final sintering temperature of 1000°C. However, for simplicity, only the results of our investigation on the phase with $x = 0.1$ will be reported in this paper.

The evolution of XRD profiles for phases derived from the metal oxalate precipitates with nominal composition $(Y_{2.9}Tb_{0.1})Al_5O_{12}$ as a function of calcination and sintering time is illustrated in Fig. 2. The products obtained from oxalate precursors after sintering at 1000°C for 12 and 16 h were found to be poorly crystalline yttrium aluminates such as $Y_4Al_2O_9$ (JCPDS file 34-368) and $YAlO_3$ (JCPDS file 16-219). Our observations are consistent with the observed sequence of formation of yttrium aluminates in the Y_2O_3–Al_2O_3 system as a function of temperature regardless of the Y_2O_3 : Al_2O_3 molar ratio described by Kinsman *et al.* (18) However, with longer heat treatment at the same temperature for 20 h the diffraction profile of as-prepared sample can clearly be identified as the YAG type structure (space group *Ia*3*d*, No. 230) and the $(Y_{2.9}Tb_{0.1})Al_5O_{12}$ phase exhibiting strong XRD intensity was obtained only after sintering at 1000°C for 24 h. The broadening of diffraction peaks reported in Fig. 2d is also a good indication of the intrinsically nano-sized nature of as-prepared YAG : Tb phases. The preparation conditions described here are apparently much milder than those generally adopted by solid-state method (7). The indexed XRD profile for $(Y_{2.9}Tb_{0.1})Al_5O_{12}$ is then shown in Fig. 2d from which the cell parameters a_o derived is 12.028(2) Å compared to 12.026(1) Å for pristine $Y_3Al_5O_{12}$. The results of our investigations on the formation of $(Y_{3-x}Tb_x)Al_5O_{12}$ solid solution with $0.05 \leq x < 3.0$ and the quenching effect of Tb^{3+} concentration on luminescence intensity have been reported elsewhere (19).

To investigate the conservation of cation stoichiometry in the process of coprecipitation, we have also carried out ICP–AES analyses on the compositions of $(Y_{2.9}Tb_{0.1})Al_5O_{12}$ samples. The typical loss of cations in the as-prepared $(Y_{2.9}Tb_{0.1})Al_5O_{12}$ sample has been determined to be $< 5.54 \times 10^{-4}$, $< 1.70 \times 10^{-2}$, and $< 9.60 \times 10^{-3}$ mol% for Tb, Y, and Al cations (19), respectively, which is considered to be not detrimental to the performance of YAG : Tb phosphors.

The bright-field TEM images showing the morphology and the size distribution of $(Y_{2.9}Tb_{0.1})Al_5O_{12}$ nanoparticles are shown in Fig. 3. In all samples of as-prepared YAG : Tb phosphor grains are aggregated and the morphology appears to be irregularly spherical or elliptical (without faceted borders) and their sizes range from 60 to 70 nm, as estimated from TEM imaging micrographs. The attempt to further reduce the grain size of YAG : Tb nanoparticles by modifying the synthetic conditions (e.g., coprecipitation pH, relative ratio of TEA/OA) is currently under investigation.

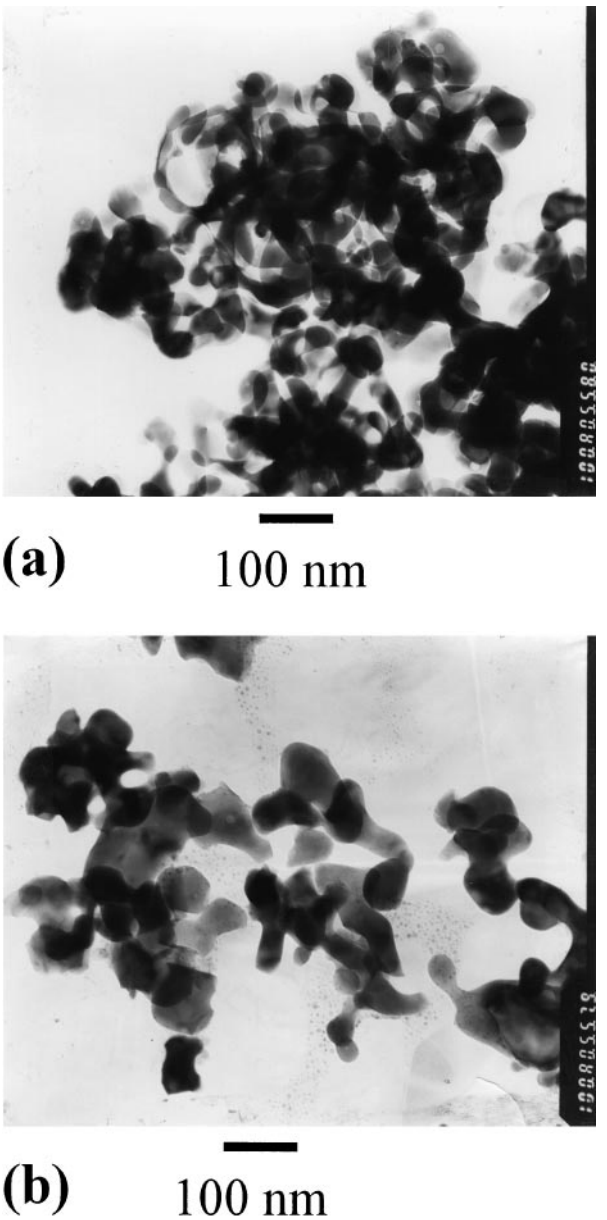

FIG. 3. Bright-field TEM images showing the morphology and the size distribution of as-prepared $(Y_{2.9}Tb_{0.1})Al_5O_{12}$ nanoparticles.

The ambient temperature photoluminescence (PL) spectrum of $(Y_{2.9}Tb_{0.1})Al_5O_{12}$ phosphor nanoparticles sintered at 1000°C for 24 h is illustrated in Fig. 4. The YAG : Tb phases are efficient green phosphors emitting a typical Tb^{3+} line spectrum under UV ($\lambda = 273$ nm) excitation. The broad excitation peak centered at 273 nm is attributed to a 4*f*–5*d*

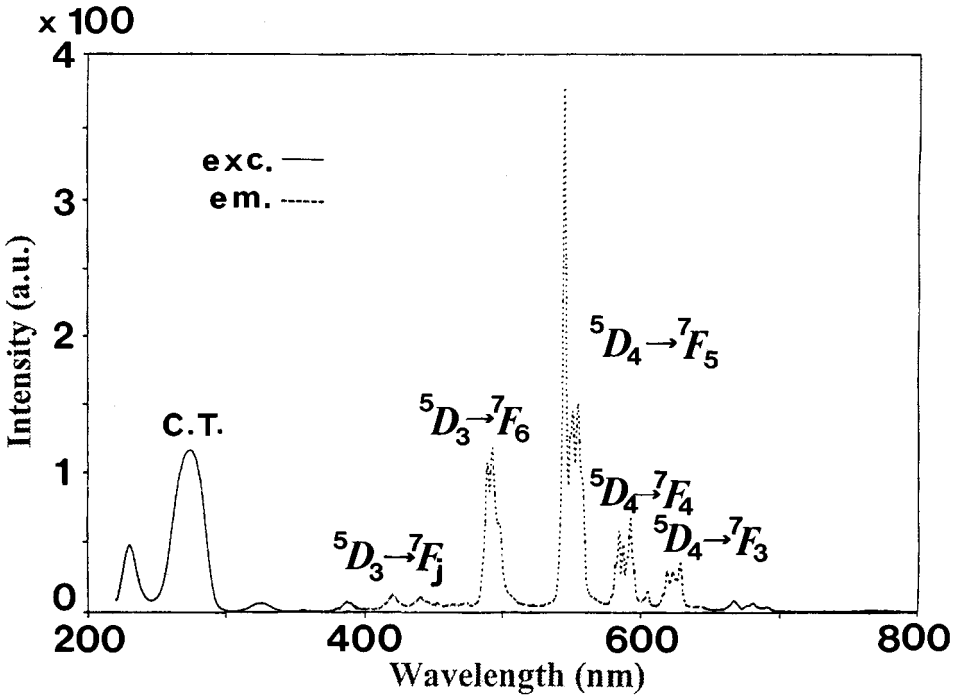

FIG. 4. Ambient temperature PL spectra of $(Y_{2.9}Tb_{0.1})Al_5O_{12}$ phosphor nanoparticles excited by UV radiation ($\lambda = 273$ nm).

charge transfer (CT) transition (20) and is followed by typical Tb^{3+} green emission. As a result of absorbing UV radiation, Tb^{3+} ion is excited to a $4f^75d$ state; it then decays stepwise from this state to the $^5D_3$ or the $^5D_4$ state which then returns to ^7F_j ($j = 3,4,5,6$) states by emitting visible light (20). No blue shift was observed in the excitation or emission PL spectra of the $(Y_{2.9}Tb_{0.1})Al_5O_{12}$ nanoparticles with respect to those of the $(Y_{2.9}Tb_{0.1})Al_5O_{12}$ phase synthesized from the solid-state route. The absence of a blue shift in the PL spectra could probably be attributed to size and agglomeration effects of the nanoparticles. The emission peaks with wavelength below 490 nm originate from the $^5D_3$ state to various $^7F_{6-3}$ ground state levels (15). At greater wavelengths the major emission peaks appearing at 545 (strongest), 586, and 622 nm are attributed to the $^5D_4$ state to $^7F_6$, $^7F_5$, and $^7F_4$, states, respectively.

CONCLUSION

Nanoparticles of YAG:Tb phosphor have been synthesized by employing an alkaline oxalate coprecipitation route at a final sintering temperature of 1000°C, which is apparently much lower than that adopted by conventional solid-state method. The grain size of as-prepared $(Y_{2.9}Tb_{0.1})Al_5O_{12}$ nanoparticles was estimated to be 60 to 70 nm, as indicated by bright-field TEM morphological studies. We found that the characteristics of ambient temperature PL spectra for $(Y_{2.9}Tb_{0.1})Al_5O_{12}$ nanoparticles is comparable to those of YAG:Tb phases synthesized via solid-state method. However, no blue shift in the excitation or emission PL spectra of the $(Y_{2.9}Tb_{0.1})Al_5O_{12}$ nanoparticles was observed.

ACKNOWLEDGMENT

We are grateful for long-term financial support from National Science Council of Taiwan, R.O.C. under Contracts NSC86-2113-M-009-006 and NSC88-2113-M-009-013. The bright-field TEM micrographs were measured at the Department of Materials Science and Engineering of NCTU.

REFERENCES

1. W. F. van der Weg, J. M. Robertson, W. K. Zwicker, and Th. J. A. Popma, *J.* Lumin. **24–25,** 633 (1981).
2. W. F. van der Weg, Th. J. A. Popma, and A. T. Vink, *J. Appl.* Phys. **57,** 5450 (1985).
3. K. Ohno and T. Abe, *J.* Electron. Soc. **141,** 1252 (1994).
4. W. R. Blumenthal and D. S. Philips, *J. Amer. Ceram. Soc.* **79,** 1047 (1996).
5. A. Ikesue, I. Furusato, and K. Kamata, *J. Amer. Ceram. Soc.* **78,** 225 (1995).
6. M. Gomi and T. Kanie, *J. Appl. Phys. Jpn.* **35,** 1789 (1996).
7. D. van der Voort, I. De Moat-Gersdorf, and G. Blasse, *Eur. J. Solid State Inorg.* Chem. **29,** 1029 (1992).
8. R. P. Rao, *J. Electrochem. Soc.* **143,** 189 (1996).
9. J. Carda and G. MoNros, *J. Solid State Chem.* **108,** 24 (1994).
10. J. M. Robertson and M. W. van Tol., *Appl. Phys. Lett.* **37,** 471 (1980).
11. Y. Liu, Z. F. Zhang, B. King, J. Halloran, and R. M. Laine, *J. Amer. Ceram. Soc.* **79,** 385 (1996).
12. P. Vaqueiro, M. P. Crosnier-Lopez, and M. A. Lopez-Quintela, *J. Solid State Chem.* **126,** 161 (1996).

13. R. N. Bhargava, D. Gallagher, X. Hong, and A. *Nurmikko*, *Phys. Rev. Lett*. **72,** 416 (1994).
14. W. P. Zhang, P. B. Xie, C. K. Duan, K. Yan, M. Yin, L. R. Lou, S. D. Xia, and J. C. Krupa, *Chem. Phys. Lett*. **292,** 133 (1998).
15. G. H. Dieke, "Spectra and Energy Levels of Rare Earth Ions in Crystals," p. 253, Wiley, New York, 1968.
16. J. P. van der Ziel, L. Kopf, and L. G. van Uitert, *Phys. Rev. B* **6,** 615 (1972).
17. D. J. Robbins, B. Cockayne, B. Lent, and J. L. Glasper, *Solid Sate Commun*. **20,** 673 (1976).
18. K. M. Kinsman, J. McKittrick, E. Sluzky, and K. Hesse, *J. Amer. Ceram. Soc*. **77,** 2866 (1994).
19. S. C. Chen, M.S. dissertation, National Chiao Tung University, Taiwan, 1997.
20. G. Blasse and A. Bril, *Philips Tech. Rev*. **31,** 304 (1970).